RSC Advances

ROYAL SOCIETY OF CHEMISTRY

www.rsc.org/advances

Journal Name

RSCPublishing

ARTICLE

Nanospheres from the self-assembly of an elastin-inspired triblock peptide

-*Cite this: DOI: 10.1039/xoxxoooooox

A. Scelsi [a,b], B. Bochicchio[a] , A. Smith[b], A. Saiani[b] and A. Pepe[a*]

Received ooth January 2012,
Accepted ooth January 2012

DOI: 10.1039/xoxxoooooox

www.rsc.org/

Peptide-based biomaterials are gaining increasing interest as biomaterials for tissue engineering as well as drug delivery systems. Many studies were conducted on amphiphilic or surfactant peptides, showing the great plethora of nanostructures that they can form, according to sequence and experimental conditions. In our work we were interested in the effect of secondary structure propensity of the peptide on the self-assembling properties. A designed peptide, having a conformation-based three-block structure, was able to form nanospheres of 100-400 nm of diameter. The molecular and supramolecular structure was investigated by several biophysical techniques and highlights the important role of conformational flexibility and π–π stacking in the self-assembly of the peptide.

Introduction

Self-assembling peptides have recently attracted significant interest due to their potential applications in nanotechnology[1-3]. Their chemical versatility and cost-effectiveness makes them ideal candidates for the design and building of functional supramolecular nanostructures for the biomaterial, drug delivery and advanced material fields[4, 5]. Many examples are described in the literature where the self-assembly is dictated by the conformation adopted by the peptides.

Alfa-helix forming peptides have been designed to form a variety of fibre morphologies[6]. In several cases, α-helical amphiphilic peptides were designed and their self-assembly determined fiber morphology driven by hydrophobic and electrostatic interactions. Coiled coil peptides, for example, in which the hydrophobic domain is created by the first and fourth residue of the heptad repeat, can form dimers, trimers, and larger aggregates, that further assemble into linked, waved, kinked or branched nanofibers[7]. However, the most studied class of self-assembling peptides are β-sheet forming peptides. In the family of *de novo* designed β-sheet peptides numerous studies have focused on amphiphatic/surfactant peptides. Amphipathic peptides have an increased propensity to self-assemble into β-sheet fibrils when their primary sequence pattern consists of alternating hydrophobic and hydrophilic amino acids. The self-assembly process is mediated through non-covalent interactions, including hydrogen bonding, van der Waals, electrostatic, and aromatic stacking interactions[6, 8]. However, the amino acid sequence patterns was also shown to exert a dramatic influence on the self-assembly propensity of the peptide, the morphology of the resulting supramolecular structure and the material properties, even when the overall hydrophobicity or charge of the related peptides are identical[9].

Another class of β-sheet rich structures are amyloid-inspired fibers, formed by peptide sequences derived from different proteins undergoing misfolding and/or misassembling and associated to pathological states of human diseases (Alzheimer Disease, diabetes). These peptides were mainly studied as model compounds to understand the factors responsible for the amyloid fibril formation, in order to develop strategies to hinder aggregation. However, interesting mechanical properties of the fibrillar[10, 11] or spherical structures[12] were detected, thus expanding the interest in these systems due to their considerable potential as novel biomaterials for nanotechnology applications.

While many studies have highlighted the role of the amino acid composition and sequence of the peptides on the self-assembly into nanostructures, focusing especially on the hydrophilic/hydrophobic compositional balance, limited studies were conducted on how secondary structure propensity can

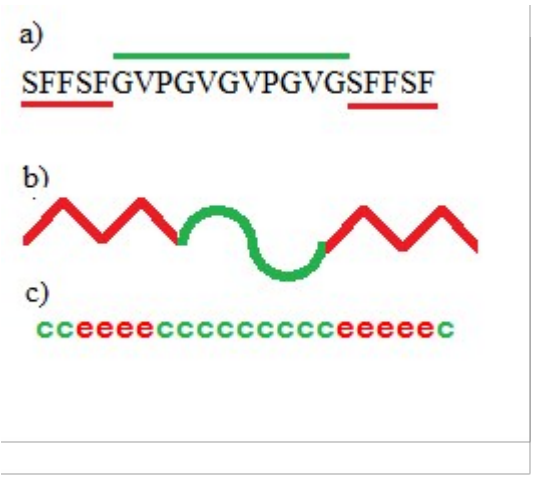

Figure1: Design of the elastin-inspired triblock SA21 peptide with indicated the conformationally different blocks: in red β-strand; in green random coil. a) peptide sequence; b) schematic representation of the conformations; c) results from GOR IV secondary structure prediction algorithm (c= random coil, e= extended β-strand).

drive or direct self-assembly of peptides into specific nanostructures. For example, the self-assembly of rod-coil co-polypeptides were reported[13-15]. However, in this case too the self-assembly is mainly driven by the amphiphilic character of the polypeptides.

An interesting class among self-assembling peptides are elastin-inspired peptides for their use in biomedical applications[16-18]. They are considered of significant importance for their low cytotoxicity, high degree of biocompatibility and tunable mechanical properties[19, 20]. Elastin-like peptides (ELP) take inspiration from the primary structure of elastin, the extracellular matrix protein conferring elasticity and resilience to organ and tissues of many vertebrates[21]. The most studied ELPs present small-sized repetitive sequences, highly enriched of hydrophobic amino acids. Elastin[22] and its soluble precursor, tropoelastin are able to form aligned and banded fibers. Interestingly, even fragments of elastin (α-elastin, κ-elastin)[23, 24] as well as many other ELPs show a peculiar self-assembly consisting of highly organized filamentous structures[22, 25, 26]. From a conformational point of view ELPs are considered intrinsically unstructured peptides that adopt in water unordered conformations in equilibrium with PPII and β-turn structures[27-29]. Even if elastin is classified as a not-globular protein, it is organized in highly ordered fibrillar structure found in ECM. This finding gives rise to the apparent "elastin paradox". In other words, it has suggested that the order found at supramolecular level, where regular fibres are observed, is generated from the disorder commonly observed at molecular level where flexible and unstructured conformations are detected thus suggesting a crucial role of the conformation for the supramolecular structure.[30, 31]

In the present study we report on the nanostructures adopted by a self-assembling three-block elastin peptide providing insight into the factors governing the self-assembly of the peptide. We show that a three-block structure, designed in order to have three blocks with β sheet-random coil-β sheet structure, shows unexpected nanospherical structures, as characterized by biophysical techniques. A complete picture of the molecular and supramolecular structure emerged pointing to the predominant role of conformational flexibility and π–π stacking on the self-assembly of the peptide.

Results and discussion

Peptide design:

The SA21 peptide was designed as an ABA three block system with two external β-sheet forming sequences, and a central flexible peptide sequence (Figure 1). The design of the peptide was inspired by two proteins able to self-assemble into peculiar nanostructures of different nature, hSAA1 and elastin. hSAA1 protein is a protein associated in serum to high density lipoproteins (HDL3), whose concentration increases during inflammation[32]. High concentration for long time, as a consequence of severe chronic inflammation states, could induce secondary systemic amyloidosis[33, 34]. Studies on different truncated peptides of hSAA1 have evidenced the fundamental role of the N-terminal region in the aggregation properties of the protein[35]. Among different fragments the SFFSF peptide, corresponding to the region 2-6 of the protein has shown a prompt β-sheet triggered self-assembly into nanofibers and nanocrystals[36].

The central region of the designed SA21 peptide contains a two-fold repeat of the consensus sequence –VGVPG– of elastin[37]. The presence of type II β-turns in the VPGV sequence is increased in less polar solution conditions (DMSO; TFE)[38]. Nevertheless, the occurrence of proline residues hinders the adoption of α-helices as well as β-sheet structures conferring high disorder to the backbone chain. As a consequence the SA21 peptide design is based on two potentially rigid β-sheet forming tracts connected by a highly flexible elastin-based central sequence (Figure 1b).

The hydrophobicity of the designed peptide is very high, considering that 57.1% of the amino acids are hydrophobic, while the other 42.9% have uncharged amino acids. The peptide sequence was submitted to the GOR4 algorithm for predicting protein secondary structure from amino acid sequence at the NPS@: Network Protein Sequence Analysis[39] website. The results are shown in figure 1c and evidenced the presence of two extended regions at the N- and C- termini while the central part is predicted to be random, in accordance with the peptide design.

Conformational studies

The secondary structure of the peptide was investigated by circular dichroism (CD) and Fourier transform infrared spectroscopy (FT-IR). Since SA21 is poorly soluble in water, hexafluoroisopropanol (HFIP) was added as co-solvent (50%) to dissolve the peptide. The CD spectrum of SA21 recorded in H_2O/HFIP (1/1, v/v) is shown in figure 2a. The spectrum recorded in the far UV region (190-250nm) shows the presence π-π* transition of the peptide bond, points toward folded

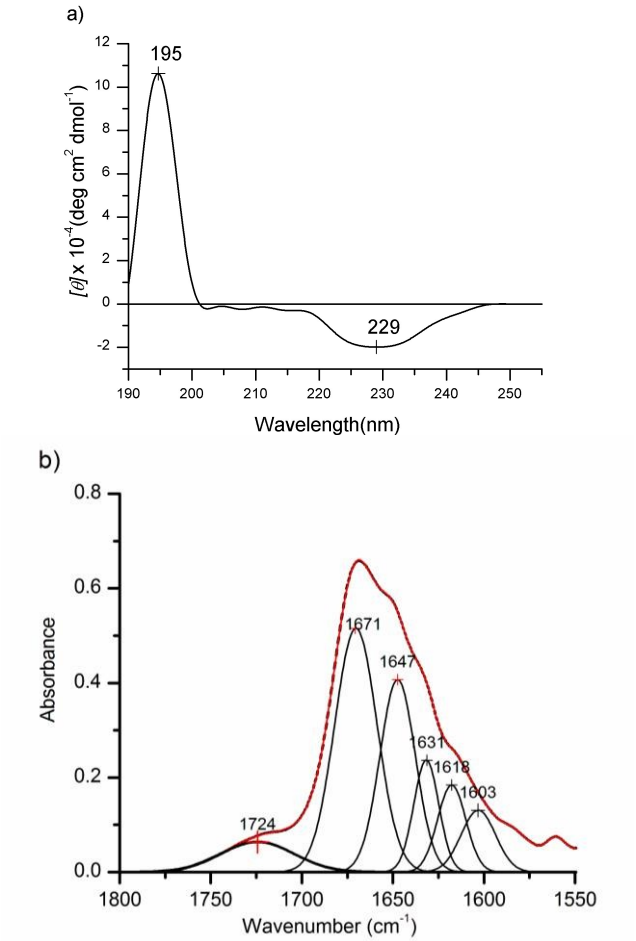

Figure 2. Conformational studies of SA21 peptide. a) Far-UV CD spectrum recorded in H_2O/HFIP (1/1) at 25°C. b) Decomposed FT-IR spectrum of the amide I' region of SA21 peptide recorded in D_2O/HFIP-d_2. The band fitting results are shown. Dashed line: experimental spectrum. Solid red line: calculated spectrum.

of an intense positive band at 195 nm, and a negative band at 230 nm. While the intense positive band at 195 nm, assigned to structures, like β-strand or β-turns, the small broad negative band at 229 nm is indicative of unordered conformations, ascribed to the central elastin-like block region. The presence of aromatic contributions associated to π–π stacking of the numerous Phe residues could be responsible for the spectral features in the 200-220 nm range. Similar contributions were observed for the FF dipeptide and for FFKLVFF peptide, involved in β-sheet promoted fibrillation[40-43].

The FT-IR spectrum was recorded on 0.5 mM SA21 peptide in D_2O/HFIP-d_2 at room temperature. The amide I' region (Figure 2b) is dominated by a band at 1671 cm^{-1} assigned to β-turn/PPII conformation. The band at 1647 cm^{-1} is usually assigned to unordered conformations, while the bands at 1631 and 1618 cm^{-1} could be assigned to H-bonded β-sheet or β–turns. The assignment of the small band at 1603 cm^{-1} is not trivial. It could be assigned to extensively dehydrated and strong intermolecular hydrogen bonded C=O bonds observed in highly aggregated proteins[44] or, alternatively, to contributions of the aromatic side chains[45].

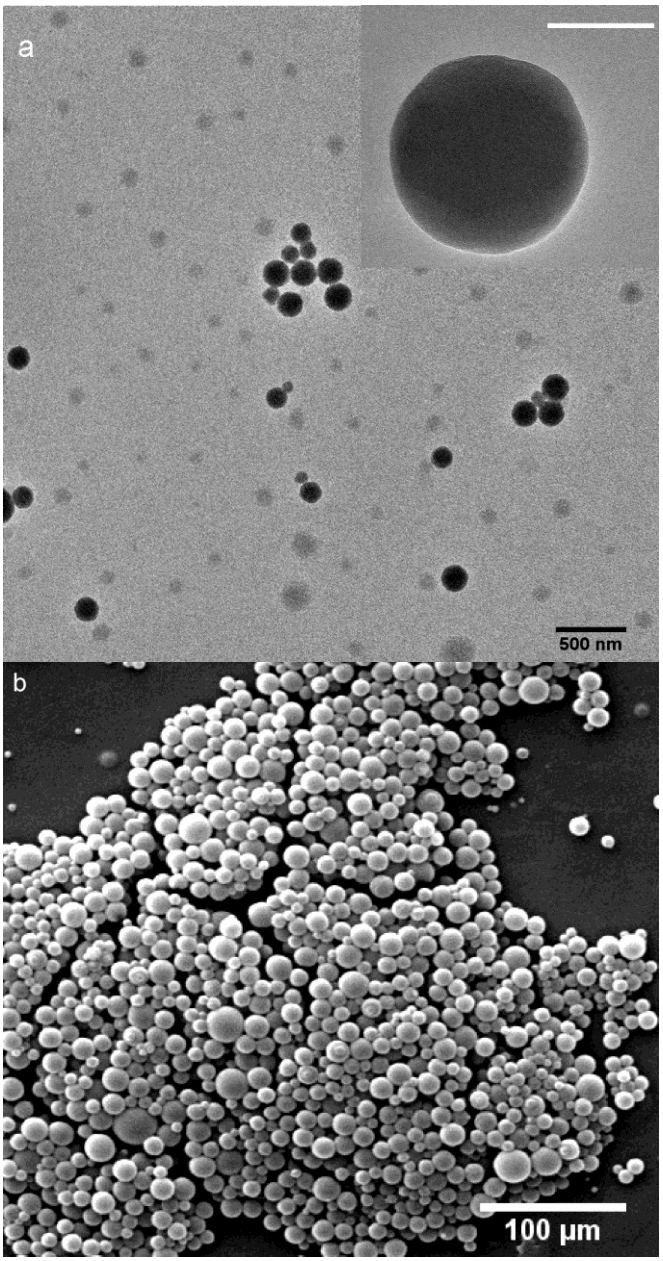

Figure 3: Representative TEM (a) and SEM (b)images of spherical nanostructures formed from SA21 peptide at 0.5 mM in H_2O/HFIP (1/1, v/v). The inset in a) represents a magnification of a nanosphere (bar =100 nm).

Supramolecular structure of SA21 peptide

The supramolecular structure of the SA21 peptide was investigated by transmission electron microscopy (TEM) and scanning electron microscopy (SEM) to probe nanoscale morphology. Few drops of the 0.5 mM solution were deposited on carbon coated grids and, after negative staining with 1% uranyl acetate, TEM images of specimen were taken (Figure 3a). The micrographies highlight the presence of isolated spherical assemblies of 100-200 nm diameter. Surprisingly, no evidence of fibrillar structures is observed despite of the presence of elastin sequences. Huge aggregates of spherical

Journal Name RSCPublishing

ARTICLE

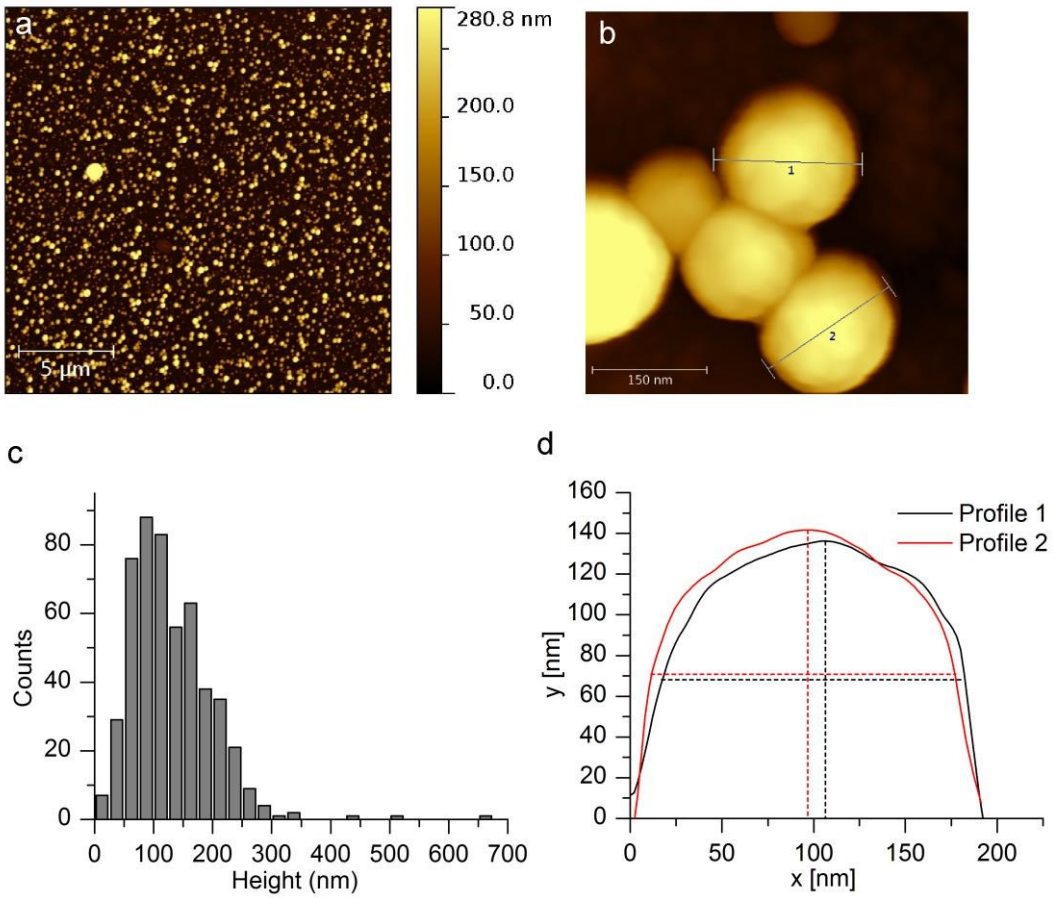

Figure 4: AFM image analysis of the SA21 peptide deposed on Si wafers. a) Topography images of an AFM image recorded in air. b) Magnification of some nanospheres, labelled with number 1 and 2 . c) Height distribution analysis of 515 nanoparticles. d) Profiles of the two nanospheres 1 and 2 shown in panel b).

nanoparticles were particularly evident when observed by SEM (Figure 3b). In order to exclude the presence of artefacts due to the high-vacuum conditions in EM analysis, and to have an independent indication about the morphology of the nanostructures, peptide self-assembled particles were also visualized by atomic force microscopy (AFM) (Figure 4). The presence of spherical structures was confirmed and a statistical analysis on the dimensions of the nanospheres was conducted. The spheres‘ height varied from 30 to 300 nm and was distributed as shown in Figure 4c. We analysed the height distribution of 515 spheres from AFM images where the spheres are evenly distributed, to assume that they are directly laying on the silicon surface. We measured the height of the spheres instead of the diameter, as the exact height of the nanostructures at the Z-range can be accurately measured by AFM, while the measurements of the lateral dimensions (*xy* plane) have an intrinsic degree of error due to the tip convolution (Figure 4d).

Role of Phe in self-assembly

The importance of aromatic side chain interactions as pivotal structural elements in the self-assembly of nanofibers/nanotubes has been discussed in many previous papers, even if the exact mechanism for aromatic stabilization is still unknown. Stacking interactions, mainly T-shaped or parallel displaced, are indicated to contribute to stability of the nanostructure[41]. Other studies have suggested that the self-assembly of aromatic peptides is mainly due to their hydrophobic character[46, 47]. To investigate the role of the aromatic interactions in nanosphere assembly of SA21 peptide, the intrinsic fluorescence of Phe was investigated (Figure 5). After excitation at 260 nm, the fluorescence emission spectrum of SA21 shows a peak at 282 nm and a more intense peak at 303 nm. The first peak shows the characteristic emission wavelength of Phe. The red shifted peak at 303 nm could be assigned to Phe residues involved in π–π stacking interactions

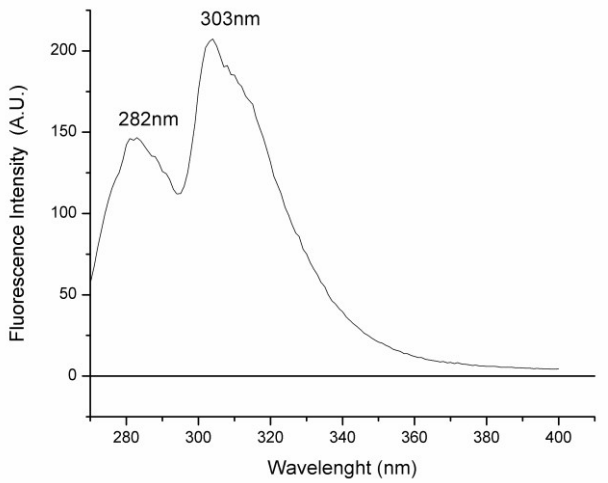

Figure 5: Intrinsic fluorescence emission spectrum of SA21 peptide recorded in H_2O/HFIP (1/1, v/v).

due to close association[48]. Previous experiments investigating intrinsic fluorescence of Phe from short peptides containing FF sequence have shown the presence of additional peaks at 303 after fibril formation[48]. The high-resolution structural models available for the FF nanotubes confirmed the close interlock of the Phe residues in the β-strands of the fibril structure. [49] However, the near-UV CD spectrum of the SA21 peptide recorded in the 250-360 nm wavelength range (Figure S1 - ESI) did not exhibit any chiroptical effect in the aromatic region, excluding that the aromatic rings are involved in rigid and fixed structures with chiral orientation, as observed for aromatic peptides forming fibers. They have rather a certain degree of freedom in the rotation of the aromatic ring of the Phe residues. The $\pi-\pi$ interactions are probably not persistent and furthermore not strengthened by backbone H-bonds, as commonly observed in fibril structures, making the nanosphere structure founded on a high number of weak and transient interactions. A validation of this hypothesis comes from the observation that on dilution and mixing we observed a reduction of the number of nanospheres and, more interestingly, an important reduction of the dimensions as observed by AFM and SEM (Figure S2 and S3-ESI). Despite dilution of the solution, the conformation of the peptide did not significantly change (Figure S4-ESI) inferring that the aggregation is reversible and not due to β-sheet promoted H-bond network of the SFFSF sequences of the peptide.

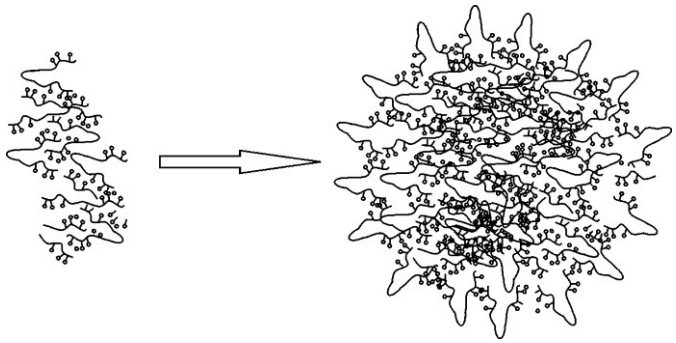

Figure 6: schematic Model of the self-assembly of the SA21 peptide in nanospheres

Role of central elastin-inspired sequence

The elastin-inspired domain of the peptide is located in the central part of the peptide and confers to this region high flexibility. The presence of significant amount of unordered/flexible conformation was shown by CD and FT-IR spectroscopy. According to recent research on unordered conformations the adoption of significant amount of transient and short regions of PPII conformation has to be considered at the basis of conformational flexibility[50, 51].

The choice of the elastin sequence in the central part of the peptides was essential for the formation of flexible loop structures. As a matter of facts the proline residues in the elastin sequence, often involved in transient β-turn structures, act as a hinge, allowing for large amplitude conformational motions[52]. A schematic representation of the proposed supramolecular model of the nanospheres is shown in Figure 6, where the presence of flexible β-turns were suggested at the basis of the bulge loop unit.

Experimental Section

Peptide synthesis and purification:

SA21 peptide was synthesized by solid phase peptide synthesis (SPPS) with a Tribute automatic peptide synthesizer (Protein Technologies Inc., Tucson, AZ, USA), using Fmoc/tBu chemistry. Fmoc-α-aminoacids were purchased from Inbios (Pozzuoli, Italy), and coupling reagent HBTU was acquired from Matrix Innovation (Quebec, Canada). Reagent used for cleavage of SA21 from resin was an aqueous solution of 95% trifluoroacetic acid (TFA, >99%). The polypeptide was purified by semipreparative reversed-phase HPLC, using binary gradient H_2O (0.1% TFA) and CH_3CN (0.1% TFA) as solvents. The purity of the peptide was assessed by HRMS (ESI) mass spectrometry (m/z 1063.52966 $[M+2H]^{2+}$, 1163.52679 calcd. for $[C_{106}H_{144}N_{21}O_{26}]^{2+}$) and ^1H NMR spectroscopy (Figure S5-ESI).

Circular dichroism (CD) spectroscopy

Circular dichroism spectra were recorded on a JASCO J-815 Spectropolarimeter (JASCO, Milan, Italy), equipped with HAAKE temperature controller. Samples were dissolved at a concentration of 0.5 mM and 0.05 mM in H_2O/HFIP (1/1, v/v)) and loaded into cylindrical quartz cells with pathlengths of 0.1mm and 1mm, respectively. Spectra were acquired in a wavelength range of 190–250 nm at room temperature, with a scan speed of 20 nm/min and a band width of 1 nm. CD spectra represented the average of 9 scans and all final spectra were obtained after subtracting the background. Data are expressed in terms of [Θ] and the molar ellipticity in units of degree cm^2

dmol^{-1}. Near–UV spectrum of the 0.5 mM peptide solution was recorded in the range 250-360 nm in the 1mm pathlength quartz cell.

FT-IR spectroscopy

SA21 peptide (0.5 mM) prepared in D_2O/HFIP-d_2 (1/1, v/v) were placed in CaF_2 cell with 500 μm path length. IR spectra were recorded on a Jasco FTIR-460 spectrometer. Each spectrum is the result of signal-averaging of 256 scans at a resolution of 2 cm^{-1} . All spectra are absorbance spectra obtained after background subtraction. Smoothing of spectra was carried out with a step of 11 or 13 data points, using the Savitzky–Golay function. Second derivatives of the spectra were obtained using a step of 13 datapoints to identify discrete absorption bands that make up the complex amide profiles. Quantitative analysis of the individual component bands of amide I was achieved by using the peak fitting module implemented in the Origins® Software (Microcalc Inc.). In the curve fitting procedure, the Voigt peak shape has been used for all peaks. The Voigt shape is a combination of the Gaussian and Lorentzian peak shapes and accounts for the broadening present in the FTIR spectrum.

TEM

SA21 (0.5 mM) was solubilized in a solution H_2O/HFIP (1/1, v/v) at room temperature. Ten μl of the solution were placed on Formvar and carbon-coated copper grids, negatively stained with a few drops of 1% uranyl acetate in bidistilled water, air-dried, and observed by transmission electron microscopy FEI-TECNAI G2 20 TWIN, operating at 100 kV.

SEM

About 10 μl of the peptide solutions were spread on silica and air-dried. The specimens were sputter-coated with gold and observed using a FEI XL30 ESEM microscope operating at 20 kV.

AFM

About 10 μl of the peptide solutions were spread on silica. Samples were stored in a Petri dish until observed by the scanning force microscope (Park Autoprobe XE-120). Specimens were observed at room temperature. Data acquisition was carried out in intermittent contact mode at scan rates between 0.4 and 3 Hz, using rectangular Si cantilevers (NCHR, Park Systems) having the radius of curvature less than 10 nm and with the nominal resonance frequency and force constant of 330 kHz and 42 N m^{-1}, respectively.

Fluorescence spectroscopy

Peptide solution at 0.5 mM concentration in H_2O/HFIP (1/1, v/v) was placed in a quartz cuvette with a 1 cm pathlength. The intrinsic fluorescence emission from Phe was measured at 25°C using Varian Cary Eclipse Fluorometer (Varian), exciting at 260 nm (slitwidth 5 nm). The emission range was 270-400 nm (slitwidth 5 nm). The scan rate was 600 nm/min and the voltage on the photomultiplier tube was set to 700V.

Conclusion

Understanding the key factors involved in the self-assembly of peptide nanostructures is critical for the rational design of bionanomaterials. In this paper we point our attention to the role played by conformations in different regions in the self-assembly of a small-sized three-block peptide. In particular, the molecular structure adopted by the peptide was correlated to the supramolecular organization. The important impact of the conformational flexibility and π–π stacking on the self-assembly of the peptide emerged. The aromatic groups generate a striking three-dimensional aromatic stacking arrangement that serves as a glue between the peptide main chains and promotes nanosphere formation. These studies strengthened the knowledge of the multiple elements (sequence, hydrophobicity, charge and conformation) ruling the self-assembly and provide general insights into biomolecular association.

Acknowledgements

The financial support from MIUR (PRIN 2010LSH3K) is gratefully acknowledged. Thanks are due to Maria Antonietta Crudele, Neluta Ibris and Alessandro Laurita (University of Basilicata) for technical assistance, AFM and EM images, respectively.

Notes and references

[a] Department of Science, University of Basilicata, Via Ateneo Lucano 10, 85100 Potenza, Italy. Fax: (+39)0971205678; Tel: (+39)0971205481; E-mail: antonietta.pepe@unibas.it

[b] School of Materials and Manchester Institute of Biotechnology, The University of Manchester, Oxford Road, Manchester, M13 9PL, U.K

† Electronic Supplementary Information (ESI) available: [Near-UV CD spectrum, Comparison of Far-UV CD spectra at two different concentration; AFM and SEM images]. See DOI: 10.1039/b000000x/

1. M. Zelzer and R. V. Ulijn, *Chem. Soc. Rev.*, 2010, **39**, 3351-3357.
2. J. H. Collier and T. Segura, *Biomaterials*, 2011, **32**, 4198-4204.
3. P. Worthington, D. J. Pochan and S. A. Langhans, *Frontiers in oncology*, 2015, **5**, 92.
4. C. A. E. Hauser and S. Zhang, *Chem. Soc. Rev.*, 2010, **39**, 2780-2790.
5. E. Gazit, *Chem. Soc. Rev.*, 2007, **36**, 1263-1269.
6. A. Saiani, A. Mohammed, H. Frielinghaus, R. Collins, N. Hodson, C. M. Kielty, M. J. Sherratt and A. F. Miller, *Soft Matter*, 2009, **5**, 193-202.
7. H. Dong, S. E. Paramonov and J. D. Hartgerink, *J. Am. Chem. Soc.*, 2008, **130**, 13691-13695.
8. C. A. Hauser and S. Zhang, *Chem Soc Rev*, 2010, **39**, 2780-2790.
9. N. R. Lee, C. J. Bowerman and B. L. Nilsson, *Biomacromolecules*, 2013, **14**, 3267-3277.
10. M. Reches and E. Gazit, *Science*, 2003, **300**, 625-627.
11. T. P. Knowles, A. W. Fitzpatrick, S. Meehan, H. R. Mott, M. Vendruscolo, C. M. Dobson and M. E. Welland, *Science*, 2007, **318**, 1900-1903.
12. L. Adler-Abramovich, N. Kol, I. Yanai, D. Barlam, R. Z. Shneck, E. Gazit and I. Rousso, *Angew. Chem. Int. Ed. Engl.*, 2010, **49**, 9939-9942.

13. E. P. Holowka, D. J. Pochan and T. J. Deming, *J. Am. Chem. Soc.*, 2005, **127**, 12423-12428.
14. Y. B. Lim, E. Lee, Y. R. Yoon, M. S. Lee and M. Lee, *Angew. Chem. Int. Ed. Engl.*, 2008, **47**, 4525-4528.
15. S. W. Jordan, C. A. Haller, R. E. Sallach, R. P. Apkarian, S. R. Hanson and E. L. Chaikof, *Biomaterials*, 2007, **28**, 1191-1197.
16. G. Pinedo-Martin, E. Castro, L. Martin, M. Alonso and J. C. Rodriguez-Cabello, *Langmuir*, 2014, **30**, 3432-3440.
17. J. E. Gagner, W. Kim and E. L. Chaikof, *Acta Biomater.*, 2014, **10**, 1542-1557.
18. S. R. MacEwan and A. Chilkoti, *Biopolymers*, 2010, **94**, 60-77.
19. A. Waterhouse, S. G. Wise, M. K. Ng and A. S. Weiss, *Tissue engineering. Part B, Reviews*, 2011, **17**, 93-99.
20. N. Annabi, S. M. Mithieux, G. Camci-Unal, M. R. Dokmeci, A. S. Weiss and A. Khademhosseini, *Biochem. Eng. J.*, 2013, **77**, 110-118.
21. J. E. Wagenseil and R. P. Mecham, *Birth Defects Res C Embryo Today*, 2007, **81**, 229-240.
22. L. Gotte, M. G. Giro, D. Volpin and R. W. Horne, *J. Ultrastruct. Res.*, 1974, **46**, 23-33.
23. B. A. Cox, B. C. Starcher and D. W. Urry, *Biochim. Biophys. Acta.*, 1973, **317**, 209-213.
24. D. Volpin, I. Pasquali-Ronchetti, D. W. Urry and L. Gotte, *J. Biol. Chem.*, 1976, **251**, 6871-6873.
25. A. Pepe, B. Bochicchio and A. M. Tamburro, *Nanomedicine*, 2007, **2**, 203-218.
26. D. Volpin and I. Pasquali-Ronchetti, *J. Ultrastruct. Res.*, 1977, **61**, 295-302.
27. A. M. Tamburro, B. Bochicchio and A. Pepe, *Biochemistry (Mosc).* 2003, **42**, 13347-13362.
28. A. M. Tamburro, B. Bochicchio and A. Pepe, *Pathol. Biol. (Paris)*, 2005, **53**, 383-389.
29. B. Bochicchio and A. Pepe, *Chirality*, 2011, **23**, 694-702.
30. A. M. Tamburro, *Nanomedicine*, 2009, **4**, 469-487.
31. L. D. Muiznieks, A. S. Weiss and F. W. Keeley, *Biochem. Cell Biol.*, 2010, **88**, 239-250.
32. G. Marhaug, *Scand. J. Immunol.*, 1983, **18**, 329-338.
33. C. M. Uhlar and A. S. Whitehead, *Eur. J. Biochem.*, 1999, **265**, 501-523.
34. G. T. Westermark and P. Westermark, *FEBS Lett.*, 2009, **583**, 2685-2690.
35. G. T. Westermark, U. Engstrom and P. Westermark, *Biochem. Biophys. Res. Commun.*, 1992, **182**, 27-33.
36. N. Rubin, E. Perugia, S. G. Wolf, E. Klein, M. Fridkin and L. Addadi, *J. Am. Chem. Soc.*, 2010, **132**, 4242-4248.
37. D. W. Urry, M. M. Long, B. A. Cox, T. Ohnishi, L. W. Mitchell and M. Jacobs, *Biochim. Biophys. Acta*, 1974, **371**, 597-602.
38. B. Bochicchio, A. Laurita, A. Heinz, C. E. Schmelzer and A. Pepe, *Biomacromolecules*, 2013, **14**, 4278-4288.
39. C. Combet, C. Blanchet, C. Geourjon and G. Deleage, *Trends Biochem. Sci.*, 2000, **25**, 147-150.
40. M. J. Krysmann, V. Castelletto, J. E. McKendrick, L. A. Clifton, I. W. Hamley, P. J. F. Harris and S. M. King, *Langmuir*, 2008, **24**, 8158-8162.
41. E. Gazit, *FASEB J.*, 2002, **16**, 77-83.
42. K. Wang, J. D. Keasling and S. J. Muller, *Int. J. Biol. Macromol.*, 2005, **36**, 232-240.
43. M. J. Krysmann, V. Castelletto, A. Kelarakis, I. W. Hamley, R. A. Hule and D. J. Pochan, *Biochemistry (Mosc).* 2008, **47**, 4597-4605.
44. M. Jackson and H. H. Mantsch, *Crit. Rev. Biochem. Mol. Biol.*, 1995, **30**, 95-120.
45. A. Barth, *Prog. Biophys. Mol. Biol.*, 2000, **74**, 141-173.
46. F. Bemporad, G. Calloni, S. Campioni, G. Plakoutsi, N. Taddei and F. Chiti, *Acc Chem Res*, 2006, **39**, 620-627.
47. S. M. Tracz, A. Abedini, M. Driscoll and D. P. Raleigh, *Biochemistry (Mosc).* 2004, **43**, 15901-15908.
48. K. E. Marshall, K. L. Morris, D. Charlton, N. O'Reilly, L. Lewis, H. Walden and L. C. Serpell, *Biochemistry (Mosc).* 2011, **50**, 2061-2071.
49. C. H. Gorbitz, *Chem Commun (Camb)*, 2006, 2332-2334.
50. R. W. Woody, *Adv. Biophys. Chem*, 1992, **2**, 37-79.
51. Z. Shi, R. W. Woody and N. R. Kallenbach, *Adv. Protein Chem.*, 2002, **62**, 163-240.
52. R. Glaves, M. Baer, E. Schreiner, R. Stoll and D. Marx, *Chemphyschem : a European journal of chemical physics and physical chemistry*, 2008, **9**, 2759-2765.